ChemPubSoc Europe

DOI: 10.1002/open.201900018

Open Access ChemistryOPEN Full Papers

Pressure-Induced Formation of Quaternary Compound and In–N Distribution in InGaAsN Zincblende from Ab Initio Calculation

Prayoonsak Pluengphon,*[a] Pornsiri Wanarattikan,[a] Thiti Bovornratanaraks,[b, c] and Burapat Inceesungvorn*[d]

We present the effects of In–N distribution and high pressure on the zincblende phase (0–5 GPa) of $In_xGa_{1-x}As_{0.963}N_{0.037}$ (x = 0.074, 0.111 and 0.148). Structural, electronic, and optical properties are analyzed, and it is found that non-isotropic distribution of In–N (type C) possesses the minimum free energy for the InGaAsN conventional cell system. An increasing indium content reduces the formation enthalpy of InGaAsN. The formation enthalpy, conduction band minimum, strength of covalent bonds, and electron density differences in free space of InGaAsN are decreased under high-pressure conditions. The dielectric performance and static permittivity of InGaAsN are lower than that of GaAs, for which the dielectric performance transforms to conductor performance at high frequency. The optimum photoabsorption coefficient is found at the composition of $In_{0.111}Ga_{0.889}As_{0.963}N_{0.037}$ (3In–N), which very well relates to the literature.

1. Introduction

In primary materials research for solar cell application, III–V binary compounds such as GaAs, InP, AlAs, and GaN have widely investigated for electronic devices and photovoltaic applications[1–6] because of having the optical band gap in range of visible light absorption. High-pressure compression in scale of gigapascal (GPa) is one of powerful methods to change the structural and electronic structures of semiconductor materials.[6–8] The crystal structures of pure and doped GaAs compounds transform from the semiconductor in zincblende structure to the semimetal phase at the 1st phase transition in the range of 7–12 GPa.[1,3] In the previous research, it was found that high-pressure condition reduces the formation enthalpy of doped III–V compounds, especially that of InP alloys.[8] Both doping and alloying methods are commonly used to improve the electronic and optical properties of III–V semiconductors to achieve the highest photoabsorption coefficient in photovoltaic process.[8–15] The quaternary III–V compounds, especially InGaAsN grown on GaAs substrate had shown high potential as the third layer in ultrahigh-efficiency multilayer photovoltaic cells.[12,13] By preparing the $In_{0.07}Ga_{0.93}As_{0.98}N_{0.02}$ thin film solar cell with 1.0 eV band gap and lattice matched to GaAs using metalorganic chemical vapor deposition, the efficiency of solar cell performance was limited by the defects or impurities from nitrogen incorporation.[14] Wei and Zunger[15] proposed that the optical bowing coefficient in GaAsN depends on giant size and composition of the diluted N concentration. The InGaAsN film on GaAs substrate gave a band gap energy suitable for long wavelength of photoluminescence in laser diodes.[16] The influence of structural nonuniformity in InGaAsN quantum wells is negligible for the luminescence efficiency.[17] The incorporation of 2–3% N concentrations into GaAs or InGaAs degraded the optical and electrical performances.[18,19] Al-Yacoub and Bellaiche[20] studied quantum mechanical effects with the perturbation theory in InGaAsN and reported that quantum coupling of electronic states and N-induced decrease the conduction band minimum and band gap of InGaAsN with respect to GaAs. Later, the optical and structural properties were enhanced when $In_{0.3}Ga_{0.7}As_{0.98}N_{0.02}$ film deposited on the InGaAs pseudo-lattice-matched substrate.[21] The incorporation of $In_{0.3}Ga_{0.7}As_{0.985}N_{0.015}$ as an absorber led to improve the static reflectivity and electron-hole recombination time due to the reduction of defect states.[22] The p-i-n structures of GaAs/InGaAsN were grown on Ge substrate by low-pressure MOVPE and it was found that the photo-current edge of InGaAsN (In = 10.3% and N = 3.3%) with 1 eV bandgap shifted to longer wavelength.[23] Study of defect distribution in InGaAsN/GaAs

[a] Dr. P. Pluengphon, Dr. P. Wanarattikan
Division of Physical Science
Faculty of Science and Technology
Huachiew Chalermprakiet University
Samutprakarn 10540, Thailand
E-mail: prayoonsak@gmail.com
[b] Dr. T. Bovornratanaraks
Extreme Conditions Physics Research Laboratory
Physics of Energy Materials Research Unit
Department of Physics, Faculty of Science
Chulalongkorn University, Bangkok 10330, Thailand
[c] Dr. T. Bovornratanaraks
Thailand Center of Excellence in Physics
Commission on Higher Education
328 Si-Ayuttaya Road, Bangkok 10400, Thailand
[d] Dr. B. Inceesungvorn
Department of Chemistry
Center of Excellence for Innovation in Chemistry (PERCH-CIC)
Center of Excellence in Materials Science and Technology
Faculty of Science, Chiang Mai University
Chiang Mai 50200, Thailand
E-mail: binceesungvorn@gmail.com

multilayer solar cells indicated that all structures showed a variety of deep energy levels with high concentrations and the electron trap state associates with a defect containing two nitrogen atoms on the lattice site.[24]

Based on the literatures, it was found that the effects of In–N distribution on electronic properties of InGaAsN under high pressure are still ambiguous and need further investigation. In this report, we therefore study the effects of In–N interaction in $In_xGa_{1-x}As_{0.963}N_{0.037}$ with the concentrations of $x=$ 0.074, 0.111 and 0.148, which relate to the ratio in experiments (In : N = 1 : 0.35 ≈ 3 : 1).[16,23] We also analyze electronic structure and photoabsorption of the InGaAsN compounds at 0 and 5 GPa. The In–N interaction and high-pressure effects on electronic and optical properties of the InGaAsN quaternary compounds are analyzed for the efficiency improvement of photovoltaic cells.

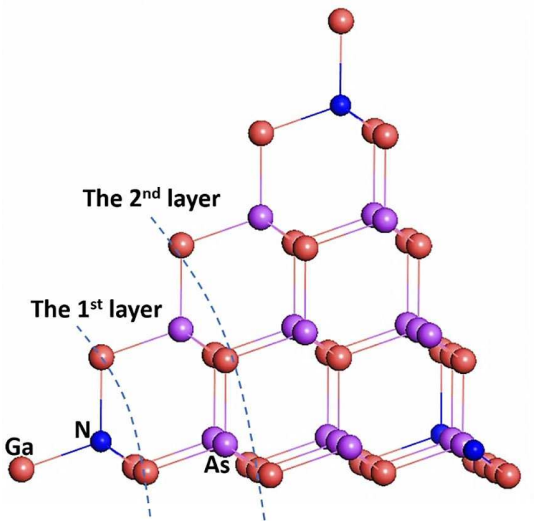

Figure 1. The 1st and 2nd layers of Ga atoms around N atom in $GaAs_{0.963}N_{0.037}$.

1.1. Computational Details

In this work, *ab initio* calculations based on density functional theory (DFT) are performed to solve the self-consistent field method as implemented in Cambridge Serial Total Energy Package (CASTEP) code.[25,26] For the quaternary compound (InGaAsN), the local density approximation schemes of Ceperley-Alder-Perdew-Zunger (LDA-CAPZ)[27] is used in the correlation functional term. By comparison of basic parameters in Table 1, the LDA result is in good agreement with the experimental result for III–V compounds, especially the lattice parameters and bulk modulus of GaAs[3] and InP.[8] To analyze the In–N distributions in $In_xGa_{1-x}As_{26}N$, the supercell (3×3×3 primitive cells of GaAs) was generated in zinc blende (ZB) structure by replacing N atom on the As sites and substituting Ga sites for In atoms (2, 3 or 4). Fractional atomic position of N is (0.083, 0.083, 0.083). It is found that the distribution of N sites in three dimensions of $GaAs_{0.963}N_{0.037}$ (or $Ga_{27}As_{26}N$) can be expressed in form triangular pyramid as shown in Figure 1. In atoms can substitute for Ga sites in the 1st and 2nd layers around N atom. The possible atomic positions of In are 4 sites (in the 1st layer) and 6 sites (in the 2nd layer) such as (0, 0, 0.333), (0, 0, 0.667) and (0.333, 0.333, 0). The quaternary compounds under investigation are $In_2Ga_{25}As_{26}N$ (2In–N), $In_3Ga_{24}As_{26}N$ (3In–N) and $In_4Ga_{23}As_{26}N$ (4In–N). These compositions correlate with the experiments[16,23] where the percentages of In and N are reported to be 10.3 and 3.3 %, respectively. The maximum energy of plane wave basis set which cooperates with ultrasoft pseudopotential[28] is used at 450 eV. Monkhorst-Pack grid sizes[29] are 3×3×3 for 27 cells and 9×9×9 for a primitive cell of GaAs-ZB. Brodyden-Fletcher-Goldfarb-Shanno (BFGS)[30] minimization scheme is used for the geometry optimization. The external pressure tensors on an optimized cell is controlled using Hellmann-Feynman theorem.[31] The BFGS optimization is completed when the total energy difference is less than 2×10^{-6} eV/atom, Hellman-Feynman forces are less than 0.006 eV/Å, the maximum ionic displacements are within 0.0002 Å, and all stress components are within 0.003 GPa.

Table 1. Comparisons on the lattice constant, bulk moduli and formation energy (F. E.) of GaAs.

Compound	a [Å]	B_0 [GPa]	F. E. [eV/f.u.]	Method
GaAs	5.65	75.40	−0.74	Exp. [32]
	5.76	77.05	−0.70	PBE + PAW [33]
	5.66	60.95	−0.70	PBE + ultrasoft [34]
	5.58	75.50	−0.71	LDA + ultrasoft (this work)
	5.74	60.30	−0.70	PBE + ultrasoft (this work)

2. Results and Discussion

2.1. In–N Distributions in ZB Phase and Free Energy of Formation

The interactions of In and N in InGaAsN were analyzed. The In atoms doping into GaAsN were classified into different types according to the number and position of atomic replacement (Figure 1 and Figure 2). All distributions for 3In–N, 2In–N and 4In–N in all types are presented in Figure 2(a), 2(b) and 2(c), respectively. In type A, all In atoms contained in the 2st layer whereas, in type B, C and D, different amount of In atoms are located in both 1st and 2nd layers as shown in Figure 2. All In–N distributions were optimized under the isotropic pressures at 0 and 5 GPa for comparisons on their physical and electronic properties. For stability of thermodynamics system, structural stability of a supercell at a given pressure can be determined using Gibbs's free energy ($G=U+PV\text{-}TS=H\text{-}TS$). The static DFT calculation was observed without thermal vibration. Therefore, Gibbs's free energy was reduced to the enthalpy of system ($H=U+PV$). Enthalpy obtained from the equation $H=E+PV$ where E is total energy or internal energy of a supercell system which calculated from Kohn-Sham equations minimization. Volume cell is incorporated in the final of geometry optimization. Pressure (P) during atomic relaxations obtained from Hellmann-

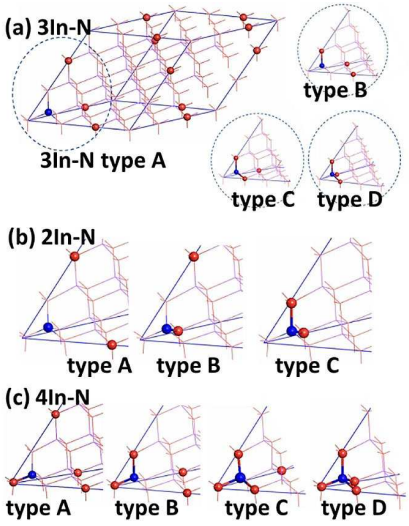

Figure 2. Atomic positions of In–N in a) $In_3Ga_{24}As_{26}N$, b) $In_2Ga_{25}As_{26}N$, and c) $In_4Ga_{23}As_{26}N$ in ZB phases.

Feynman theorem and the third-order Birch–Murnaghan equation of state. Free energy difference or relative enthalpies (H–H_A) as shown in Table 2 were calculated from enthalpy difference between the considered structure (H) and structure type A in the same composition (H_A). Stability of three compositions (2In–N, 3In–N and 4In–N) can be determined by formation enthalpy (H_f)[35,36] expressed as Equation (1):

$$H_f = H_{In_xGa_{27-x}As_{26}N} - \left[H_{27GaAs} + xH_{In,solid} + H_{N,solid} - xH_{Ga,solid} - H_{As,solid}\right] \quad (1)$$

where $H_{In_xGa_{27-x}As_{26}N}$ and $H_{27GaAs}$are the enthalpies of $In_xGa_{27-x}As_{26}N$ and 27cells of GaAs.

$H_{In,solid}$, $H_{N,solid}$, $H_{Ga,solid}$and $H_{As,solid}$ are the enthalpies in solid forms of In, N, Ga and As, respectively. According to Table 1, the basic parameters and H_f of GaAs and GaAsN found in this work are comparable to those in previous studies,[32–34] indicating the reliability of our calculation results. In Table 2, the enthalpy differences (H–H_A) were calculated with the systematic error of ±0.02 eV. We found that k-point set started to finite at 2×2×2 for $Ga_{27}As_{26}N$. The systematic error of total energy calculation is 0.02 eV/f. u. when compared with the k-point set 5×5×5, while the difference energy value between types A, B, C and D in Table 2 are in the range of 0.08–1.38 eV, which is larger than systematic error. Therefore, the 3×3×3 k-point, which is used in our calculations, is valid for comparison. H_A values per formula unit are −2178.92 eV (3In–N at 0 GPa), −2177.60 eV (3In–N at 5 GPa), −2197.19 eV (2In–N at 0 GPa), −2195.88 eV (2In–N at 5 GPa), −2160.66 eV (4In–N at 0 GPa) and −2159.33 eV (4In–N at 5 GPa), respectively. We found that the minimum free energies, indicating the most stable structures, of all compounds (2In–N, 3In–N and 4In–N) appeared in type C (Figure 2) in both 0 and 5 GPa. The results showed that both isotopic (type D of 4In–N) and random (type A of 3In–N and 2In–N) configurations aren't the most stable structure for InGaAsN. Upon considering the formation enthalpy, the stability of structures with different In:N ratios is in the following order; 2In–N > 3In–N > 4In–N. An increased energy barrier in formation process is found to be proportional to In concentration due to high potential originated from the larger size of In than Ga atom. As seen from Table 2, high pressure (5 GPa) also reduces the formation energy of InGaAsN in ZB phase compared to that at ambient condition. These are very well in agreement with those observed in the III–V (InP) alloys system from the previous work.[8] Although the free energies of GaAsN system increased under an external stress, the energy barriers of In substitution in the host GaAsN reduced under the increasing pressure.

2.2. Electronic Structure and Chemical Bonds

After the structures of 2In–N, 3In–N and 4In–N were optimized, their electronic structures in terms of band structure and density of states (DOSs) can be obtained from the solution of Kohn-Sham Hamiltonian in the 1st Brillouin zone. The DOSs of the most stable (type C) compounds and pure GaAs in Figure 3(a) indicated that the band gap of InGaAsN alloys decreases with respect to pure GaAs, supporting the previous studies.[14–15,20] Conduction band minimum (CBM) of InGaAsN shifts downward to valence band maximum (VBM) which corresponds to the previous report of quantum couplings between the CBM and other electronic states of pure GaAs and N-induced effect.[20] The bandgap of InGaAsN shifts to the longer wavelength when compared with GaAs.[23] An increasing amount of In atom in InGaAsN decrease both band gap and CBM level in the following trend: 4In–N < 3In–N < 2In–N < GaAs. For DOSs of 2In–N and 3In–N at 0 and 5 GPa in Figure 3(b–d), the results show that the distribution of In atoms

Table 2. The relative and formation enthalpies of 2In–N, 3In–N and 4In–N at 0 and 5 GPa.

Enthalpy [eV/cell]	Compound Type\pressure	2In-N 0 GPa	5 GPa	3In-N 0 GPa	5 GPa	4In-N 0 GPa	5 GPa
Relative	A	0.00	0.00	0.00	0.00	0.00	0.00
(H–H_A)	B	−0.25	−0.27	−0.23	−0.32	−0.30	−0.31
	C	−0.36	−0.36	−0.55	−0.70	−0.49	−0.46
	D	–	–	0.17	−0.49	−0.44	−0.42
Formation	A	−0.75	−1.02	−0.27	−0.57	0.08	−0.22
(H_f)	B	−1.00	−1.30	−0.50	−-0.89	−0.22	−0.52
	C	−1.11	−1.38	−0.81	−1.27	−0.41	−0.68
	D	–	–	−0.10	−1.06	−0.36	−0.64

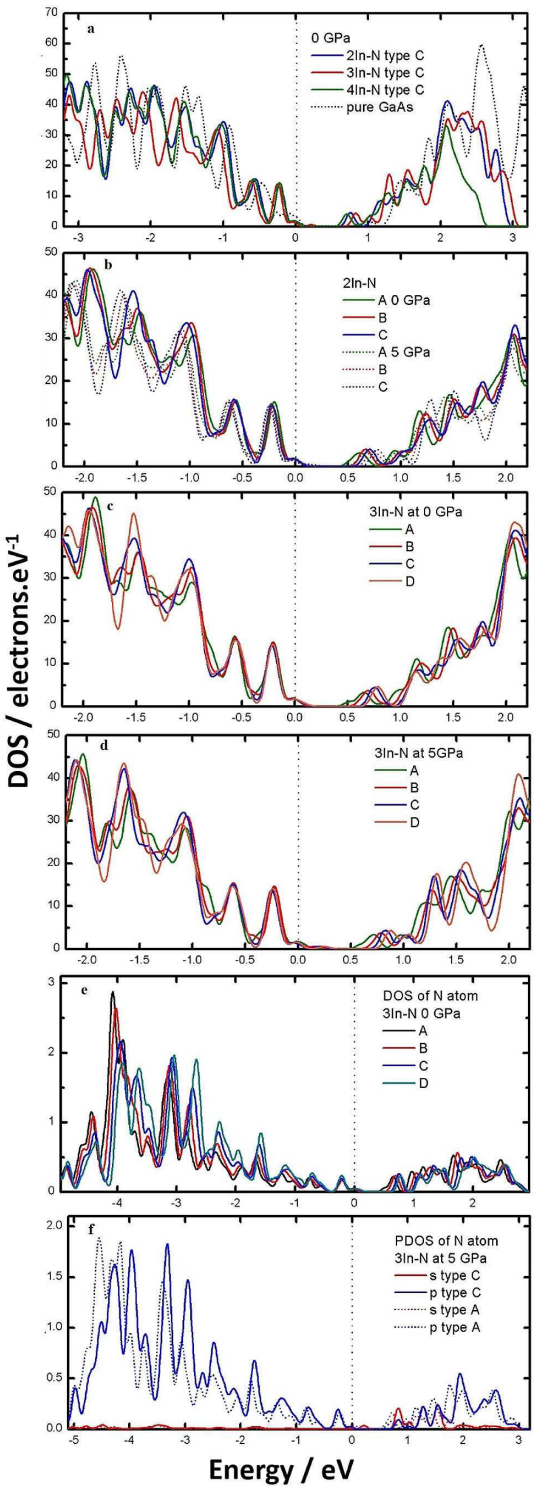

Figure 3. The DOSs of a) type C and GaAs at 0 GPa, b) 2In–N at 0 and 5 GPa, c) 3In–N at 0 GPa, d) 3In–N at 5 GPa, e) N atom in 3In–N at 0 GPa and f) PDOSs of N atom in 3In–N at 0 GPa.

in the 2nd layer in type A reduces the CBM level more than that in the 1st layer near N atom. DOSs of N atom in 3In–N in Figure 3(e) illustrate that narrow band gap in type A incorporates with total DOSs. Partial density of states (PDOSs) of N atom in 3In–N compound in Figure 3(f) show that *s* orbital is a main available state at CBM while *p* orbital is a main occupied state at VBM. In Figure 4, the surface contour plot represents

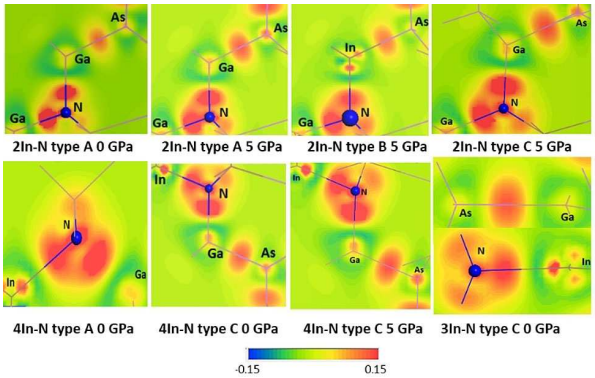

Figure 4. Electron density differences of InGaAsN alloys in the range of −0.15 to 0.15 in unit of electrons per cubic bohr.

the electron density difference (EDD) of InGaAsN compounds in high-symmetry plane. The EDD contour plot indicates the strength of chemical bonds and the relative quantity of sharing electrons in space, which calculated from the difference of electron densities in solid form and isolated atoms. Colors in contour plots represent the values of EDD in the range of −0.15 (blue zone) and 0.15 (red zone). High pressure at 5 GPa increases the strength of chemical bonds and density of sharing electrons in space because bond lengths in ZB phase are pressed in three dimensions. High pressure induces available states in both conduction and valence bands that extend along E-axis. In Tabl 3, the decreasing of bond lengths induces the excited states which relate to the extended area of DOS function. When In atom substitutes for Ga site, the positive EDD (red zone) reduces in space and condenses at In site. EDD around N atom increases because of high-electronegativity of N element. We can conclude that the In substitution reduces the strength of covalent bonds and the sharing electrons in space. Order of the average In–N bond lengths is found to be: A > B > C > D. For comparisons on the bond lengths, In–As bond is longer than Ga–As bond and In–N bond is longer than Ga–N bond, which relate to the order of atomic size (In > Ga) in the periodic table.

2.3. Photoabsorption Coefficients

The optical properties and photoabsorption coefficients of InGaAsN alloys were also analyzed and compared to obtain a suitable condition for photovoltaic application. All optical properties from DFT were evaluated from the real (R) and Imaginary (Im) parts of dielectric function through the Kramers-Kronig relations.[37,38] The Imaginary part of dielectric function is proportional to a probability of transition states of carriers from VBM up to CBM, which stimulated by the external photon energy sources.

In Figure 5(a), the calculated dielectric functions both real (ε_1) and imaginary (ε_2) parts are compared with the previous experiment which presented in the frequency range of 0.5–6.0 eV.[5] Although the calculated imaginary part at 0–3 eV has shifted to low frequency compared with that from experiment due to the narrow band gap from LDA calculation,[39] the trends of graphs are in consistent with the experimental finding.[5] To study the optical properties in the doped GaAs system, the LDA result was compared to the sX-LDA hybrid-functional in previous our report.[39] Although sX-LDA improves bandgap from LDA, they have the same tendency of photoabsorption in the doped GaAs.

At 5 GPa, the calculated imaginary part shifts to positive frequency (+x axis) because band gaps of GaAs[3] and their alloy increase under high pressure in ZB phase (0–7 GPa). The imaginary part relates to probability of transition states of carriers from VBM to CBM. In Figure 5(b), probability of transition states in 3In–N is higher than that of 2In–N and 4In–N. In addition, the real part of dielectric function relates to the stored energy within the medium. At low-frequency limit, dielectric function as a constant is the response of a medium to static electric fields that called the static permittivity. The imaginary part is dominated at low-frequency limit. Both alloy and pressure effects reduce the dielectric performance due to the decreasing of $\varepsilon_2/\varepsilon_1$ ratio. InGaAsN reduces static permittivity from the host GaAs.

Photoabsorption coefficient obtained from the Kramers-Kronig relations [Eq. (2)]:

$$I(\omega) = 2\omega\left(\frac{\sqrt{\varepsilon_1^2(\omega)+\varepsilon_2^2(\omega)}-\varepsilon_1(\omega)}{2}\right)^{1/2}. \quad (2)$$

Photoabsorptions of InGaAsN alloys at 0 and 5 GPa in the visible light wavelength are illustrated in Figure 6. The results indicate that photoabsorption coefficients of the alloys in ZB decrease with the increasing of pressure. However, the InGaAsN alloys give the better solution for photovoltaic cell due to high absorption coefficient in the visible light region. The 3In–N compound gives the optimum solution when compared with 2In–N and 4In–N, which is in consistent with the experimental investigations.[16,23] Absorption coefficients of all types (A, B, C and D) are reduced at high pressure (5 GPa) because of the increasing band gap and decreasing of EDOSs peaks at VBM and CBM.

3. Conclusions

The In–N interactions effect on structural, electronic and optical properties of $In_xGa_{1-x}As_{0.963}N_{0.037}$ (x = 0.074, 0.111 and 0.148) in ZB phase at 0 and 5 GPa have been investigated in this work. It is found that the In–N distribution in type C is the most stable distribution for 2In–N, 3In–N and 4In–N compositions. Structural stability of alloys with different In concentrations considered based on the formation enthalpy is found as follows: 2In–N > 3In–N > 4In–N. Based on electronic structure calculation, the energy of formation process increases with the In concentration in GaAsN, but decreases when increasing pressure to 5 GPa. The In substitution reduces band gap and

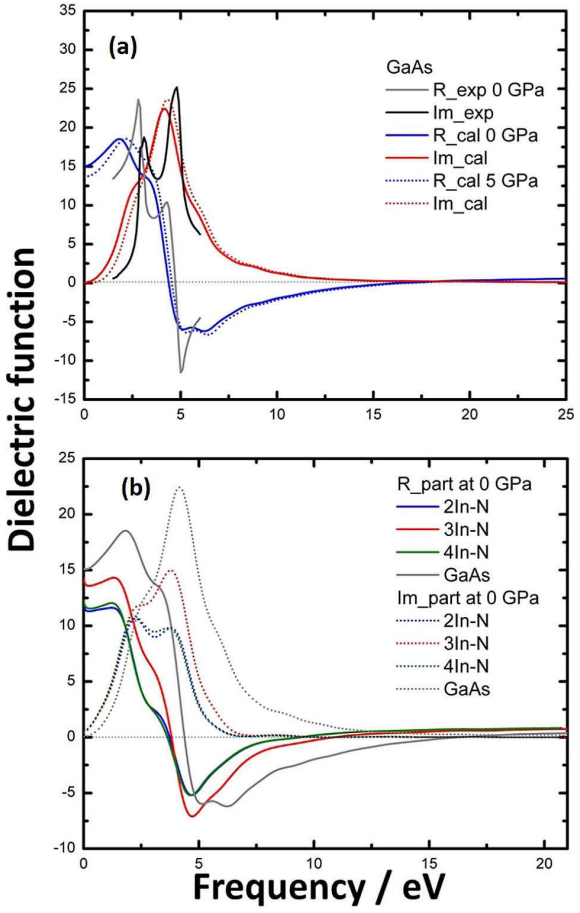

Figure 5. The calculated dielectric functions in real (R) and imaginary (Im) parts of a) GaAs at 0 and 5 GPa compared with previous experiment;[5] b) 2In–N, 3In–N and 4In–N at 0 GPa.

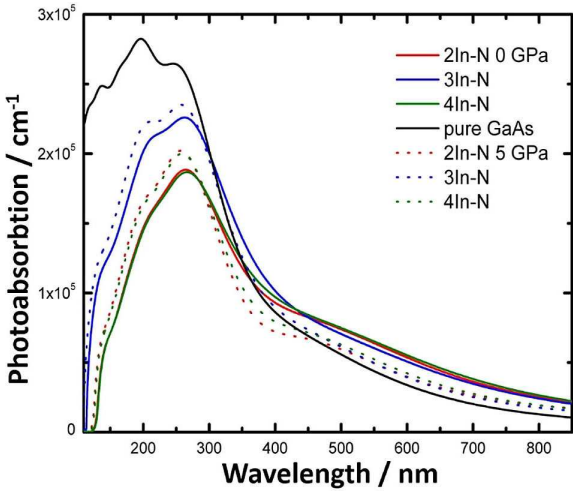

Figure 6. Photoabsorption of InGaAsN alloys at 0 and 5 GPa compared with pure GaAs at 0 GPa.

Table 3. Average bond lengths around N in InGaAsN under pressure (– represented "no bonding").

Structure	*P* [GPa])	Bond length [Å] in types A, B, C, D Ga-As	Ga-N	In-N	In-As
2In–N	0	2.44, 2.40, 2.41	2.04,2.02, 1.99	–, 2.27, 2.23	2.54, 2.57, 2.60
	5	2.39, 2.35, 2.40	2.00, 1.98, 1.96	–, 2.22, 2.19	2.53, 2.54, 2.55
3In–N	0	2.43, 2.42, 2.40, 2.41	2.03, 2.01, 1.99, 1.96	–, 2.27, 2.24, 2.21	2.56, 2.57, 2.60, 2.59
	5	2.38, 2.37, 2.37, 3.36	2.00, 1.98, 1.95, 1.93	–, 2.22, 2.20, 2.17	2.51, 2.52, 2.54, 2.54
4In–N	0	2.41, 2.42, 2.43, 2.40	2.02, 1.99, 1.96, –	2.23, 2.20, 2.20, 2.18	2.57, 2.57, 2.58, 2.59
	5	2.37, 2.37, 2.39, 2.36	1.99, 1.96, 1.93, –	2.19, 2.19, 2.17, 2.14	2.51, 2.56, 2.54, 2.54

CBM level in the following order: 4In–N < 3In–N < 2In–N < GaAs. Additionally, the presence of In atoms in the 2nd layer of type A reduces the CBM level. The PDOSs of N atom showed that *s* orbital is a main occupied state at CBM while *p* orbital is a main unoccupied state at VBM. Moreover, the In impurity reduces the bond strength and electron density in space. Photoabsorption coefficient of InGaAsN alloys in ZB also decreases when increasing pressure. Among different In : N ratio in InGaAsN, the 3In : N gives the optimum absorption coefficient compared with 2In–N and 4In–N.

Acknowledgements

This work has been partially supported by Chiang Mai University, National Research Council of Thailand, the Center of Excellence in Materials Science and Technology, the Center for Innovation in Chemistry (PERCH-CIC), Commission on Higher Education, Ministry of Education. Computing facilities have been supported by Super SCI-IV research grant, Faculty of Science and Ratchadaphiseksomphot Endowment Fund of Chulalongkorn University. P. P. would like to acknowledge the financial supports and facilities from Huachiew Chalermprakiet University and Thailand Research Fund (TRF) MRG6080231.

Conflict of Interest

The authors declare no conflict of interest.

Keywords: structural stability · electronic structure · quaternary alloy · photoabsorption

[1] J. Wang, B. Wu, G. Zhang, L. Tian, G. Gu, C. Gao, *RSC Adv.* **2016**, *6*, 10144–10149.
[2] N. Bouarissa, *Physica B* **2011**, *406*, 2583–2587.
[3] P. Pluengphon, T. Bovornratanaraks, S. Vannarat, U. Pinsook, *Solid State Commun.* **2014**, *195*, 26–30.
[4] C. Liu, M. Ma, X. Yuan, H. Sun, P. Ying, *Comput. Mater. Sci.* **2017**, *128*, 337–342.
[5] D. E. Aspnes, A. A. Studna, *Phys. Rev. B* **1983**, *27*, 985–1009.
[6] A. Abdollahi, M. M. Golzan, K. Aghayar, *Comput. Mater. Sci.* **2016**, *120*, 70–76.
[7] Y. H. R. Chang, T. L. Yoon, T. L. Lim, M. H. Tuh, *J. Alloys Compd.* **2017**, *704*, 160–169.
[8] P. Pluengphon, T. Bovornratanaraks, U. Pinsook, *J. Alloys Compd.* **2017**, *700*, 98–105.
[9] S. Li, H. Qiu, C. Wang, Y. Sun, X. Du, J. Zhao, *Sol. Energy Mater. Sol. Cells* **2016**, *149*, 97–102.
[10] T. Tanaka, T. Terasawa, Y. Okano, S. Tsutsumi, K. Saito, Q. Guo, *Sol. Energy Mater. Sol. Cells* **2017**, *169*, 1–7.
[11] H. Huang, C. Yang, M. Wang, X. Ma, *Sol. Energy Mater. Sol. Cells* **2017**, *170*, 233–238.
[12] D. J. Friedman, J. F. Geisz, S. R. Kurtz, J. M. Olson, *J. Cryst. Growth* **1998**, *195*, 409–416.
[13] S. R. Kurtz, D. Myers, J. M. Olsen, *IEEE Photovoltaic Spec. Conf., 26th* (New York) **1997**, p. 875.
[14] S. R. Kurtz, A. A. Allerman, E. D. Jones, J. M. Gee, J. J. Banas, B. E. Hammons, *Appl. Phys. Lett.* **1999**, *74*, 729–731.
[15] S. H. Wei, A. Zunger, *Phys. Rev. Lett.* **1996**, *76*, 664–667.
[16] M. Kondow, K. Uomi, A. Niwa, T. Kitatani, S. Watahaki, Y. Yazawa, *Jpn. J. Appl. Phys.* **1996**, *35*, 1273–1275.
[17] L. Geelhaar, M. Galluppi, G. Jaschke, R. Averbeck, H. Riechert, T. Remmele, *Appl. Phys. Lett.* **2006**, *88*, 011903.
[18] S. Sanorpim, F. Nakajima, W. Ono, R. Katayama, K. Onabe, *Phys. Status Solidi A* **2006**, *203*, 1612–1617.
[19] S. R. Kurtz, A. A. Allerman, C. H. Seager, R. M. Sieg, E. D. Jones, *Appl. Phys. Lett.* **2000**, *77*, 400–402.
[20] A. Al-Yacoub, L. Bellaiche, *Phys. Rev. B* **2000**, *62*, 10847–10851.
[21] P. Kongjaeng, S. Sanorpim, T. Yamamoto, W. Ono, F. Nakajima, R. Katayama, K. Onabe, *J. Cryst. Growth* **2007**, *298*, 111–115.
[22] F. Schättiger, D. Bauer, J. Demsar, T. Dekorsy, J. Kleinbauer, *Appl. Phys. B* **2012**, *106*, 605–612.
[23] K. Uesugi, S. Kuboya, S. Sanorpim, K. Onabe, *Phys. Status Solidi C* **2014**, *11*, 561–564.
[24] A. Kosa, L. Stuchlikova, L. Harmatha, M. Mikolasek, J. Kovac *Sol. Energy* **2016**, *132*, 587–590.
[25] M. C. Payne, M. P. Teter, D. C. Allan, T. A. Arias, J. D. Joannopoulos, *Rev. Mod. Phys.* **1992**, *64*, 1045–1097.
[26] M. D. Segall, P. L. D. Lindan, M. J. Probert, C. J. Pickard, P. J. Hasnip, *J. Phys. Condens. Matter* **2002**, *14*, 2717–2744.
[27] J. P. Perdew, A. Zunger, *Phys. Rev. B* **1981**, *23*, 5048–5079.
[28] D. Vanderbilt, *Phys. Rev. B* **1990**, *41*, 7892–7895.
[29] H. J. Monkhorst, J. D. Pack, *Phys. Rev. B* **1976**, *13*, 5188–5192.
[30] B. G. Pfommer, M. Cote, S. G. Louie, M. L. Cohen, *J. Comput. Phys.* **1997**, *131*, 233–240.
[31] R. P. Feynman, *Phys. Rev.* **1939**, *56*, 340–343.
[32] W. M. Haynes, CRC Handbook of Chemistry and Physics, 92nd ed. (CRC Press, **2012**).
[33] H. A. Tahini, A. Chroneos, S. T. Murphy, U. Schwingenschlögl, R. W. Grimes, *J. Appl. Phys.* **2013**, *114*, 063517.
[34] N. Martínez, J. A. R. Martínez, *J. Phys. Conf. Ser.* **2016**, *743*, 012007.
[35] M. Aslan, B. G. Yalcın, M. Ustundag, *J. Alloys Compd.* **2012**, *519*, 55–59.
[36] Z. Y. Jiao, T. X. Wang, S. H. Ma, *J. Alloys Compd.* **2016**, *687*, 47–53.
[37] R. F. Egerton, *Electron Energy-loss Spectroscopy in the Electron Microscope*, second ed. (Plenum Press, New York, **1996**).
[38] M. Schönleber, D. Klotz, E. Ivers-Tiffée, *Electrochim. Acta* **2014**, *131*, 20–27.
[39] P. Pluengphon, T. Bovornratanaraks, S. Vannarat, U. Pinsook, *Solid State Commun.* **2015**, *202*, 19–23.

Manuscript received: January 14, 2019
Revised manuscript received: February 18, 2019